KJPP

Original Article

3,3′,4,4′-tetrachlorobiphenyl (PCB77) enhances human Kv1.3 channel currents and alters cytokine production

Jong-Hui Kim[1,2,#], Soobeen Hwang[1,2,#], Seo-In Park[1,2], Hyo-Ji Lee[3], Yu-Jin Jung[2,3], and Su-Hyun Jo[1,2,*]

[1]Department of Physiology, Institute of Bioscience and Biotechnology, Kangwon National University School of Medicine, [2]Interdisciplinary Graduate Program in BIT Medical Convergence, [3]Department of Biological Sciences and Kangwon Radiation Convergence Research Support Center, Kangwon National University, Chuncheon 24341, Korea

ABSTRACT Polychlorinated biphenyls (PCBs) were once used throughout various industries; however, because of their persistence in the environment, exposure remains a global threat to the environment and human health. The Kv1.3 and Kv1.5 channels have been implicated in the immunotoxicity and cardiotoxicity of PCBs, respectively. We determined whether 3,3′,4,4′-tetrachlorobiphenyl (PCB77), a dioxin-like PCB, alters human Kv1.3 and Kv1.5 currents using the *Xenopus* oocyte expression system. Exposure to 10 nM PCB77 for 15 min enhanced the Kv1.3 current by approximately 30.6%, whereas PCB77 did not affect the Kv1.5 current at concentrations up to 10 nM. This increase in the Kv1.3 current was associated with slower activation and inactivation kinetics as well as right-shifting of the steady-state activation curve. Pretreatment with PCB77 significantly suppressed tumor necrosis factor-α and interleukin-10 production in lipopolysaccharide-stimulated Raw264.7 macrophages. Overall, these data suggest that acute exposure to trace concentrations of PCB77 impairs immune function, possibly by enhancing Kv1.3 currents.

INTRODUCTION

Polychlorinated biphenyls (PCBs) were once manufactured in large quantities for use as lubricants, coolants, hydraulic and dielectric fluids, as well as numerous other purposes; however, their production was banned in most countries since the 1970s because of their harmful effects, such as neurotoxicity, hepatotoxicity, endocrine disruption, and carcinogenicity on wildlife and humans [1]. The PCB backbone consists of two six-carbon rings linked by a single carbon bond, with 209 possible chlorinated congeners [2]. Highly chlorinated congeners are extremely insoluble in water [3], which may partially explain the resistance of these compounds to biodegradation and their tendency to accumulate in fatty tissues [3]. Toxicity to various organs have been reported due to the ac-

cumulation of PCBs in animal and the human body [1], and even after their use was banned in the 1970s, this risk is difficult to eliminate.

Exposure to highly chlorinated PCB congeners can impair the function of the immune and nervous systems, increase the incidence of cancer, and disrupt *in utero* development [4-7]. Furthermore, PCB congeners with four or more chlorines are potent activators of the aryl hydrocarbon receptor (AhR), an important regulator of the metabolic and immune responses to environmental stressors [2]. Various PCB congeners can exhibit unique biological effects [5], which requires the examination of each PCB individually. In this study, we examined the effects of 3,3′,4,4′-tetrachlorobiphenyl (PCB77) (Fig. 1), a dioxin-like PCB (DL-PCB) with four chlorines in its planar structure [7]. It has been
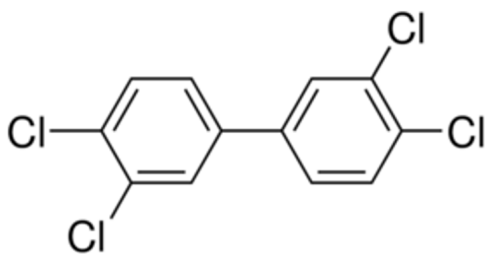
Fig. 1. Structure of 3,3′,4,4′-tetrachlorobiphenyl (PCB 77).

shown to reduce thyroid function [6], increase the risk of uterine and breast tumors [8], suppress humoral and cellular immunity through AhR activation [9,10], and impair immune function by inhibiting cytotoxic T-cell activity and antibody production [11,12].

The voltage-dependent K$^+$ (Kv) channels are a superfamily consisting of 12 subfamilies (Kv1–Kv12) that contribute to a myriad of physiological processes, including immune function, cell volume regulation, apoptosis, and differentiation, by dynamically modulating membrane potentials, electrophysiological responses to stimulation, calcium signaling, and intracellular osmolarity [13,14]. The Kv channels, Kv1.3 and Kv1.5, are members of the Kv1 Shaker family and have been implicated in tissue differentiation and cell proliferation [15]. The Kv1.5 channel is predominantly expressed in the heart and pancreatic β-cells [16,17]. In human atrial muscle cells, these channels mediate ultra-rapid delayed rectifier K$^+$ currents that contribute to action potential repolarization [18]. A loss of function causes prolongation of the action potential, and early after depolarization in human atrial myocytes, their vulnerability to stress-triggered fibrillation increases [19].

The Kv1.3 channel is encoded by the *KCNA3* gene [20] and is primarily expressed in neurons of the hypothalamus and olfactory bulb, T and B cells, microglia, dendritic cells, and macrophages [21]. Kv1.3 channels appear to play a role in switching normally quiescent cells into a proliferative state [22]. For example, surface Kv1.3 channels regulate the activation and proliferation of T cells by controlling membrane potential and Ca^{2+} signaling [23,24]. In addition to T cells, Kv1.3 channels are expressed in macrophages, osteoclasts, platelets, B cells, and kidney cells [25,26]. In macrophages and neutrophils, Kv1.3 channels regulate phagocytic activity, the inflammatory response, and migration/invasion [22]. Dysregulation of these functions is associated with chronic inflammatory diseases. Zhu *et al*. [27] reported that the selective pharmacological blockade of Kv1.3 channels with ShK enhances phagocytosis and nitric oxide production in Raw264.7 macrophages. Another study found that the potent inflammation activator lipopolysaccharide (LPS) upregulates the transcriptional and translational levels of Kv1.3 channels and proinflammatory cytokines, including interleukin-1β (IL-1β) and tumor necrosis factor-α (TNF-α), whereas Kv1.3 KO decreases these responses [28].

In this study, we examined the effects of PCB77 on human Kv1.3 and Kv1.5 currents expressed in *Xenopus* oocytes using two-microelectrode voltage clamping and the effects on the Kv1.3 channel and cytokine production in LPS-treated macrophages. Collectively, these findings suggest that PCB77 inhibits macrophage activity by upregulating Kv1.3-mediated currents.

METHODS

Expression of Kv1.3 and Kv1.5 in oocytes

Complementary RNAs encoding human Kv1.3 (hKv 1.3; GenBank accession no. BC035059.1) and Kv1.5 (hKv 1.5, GenBank: BC099665.3) were synthesized *via in vitro* transcription using Message Machine T7 kits (Ambion). They were stored in nuclease-free water at −80°C. Stage V and VI oocytes were surgically harvested from female *Xenopus laevis* (Nasco or the Korean *Xenopus* Resource Center for Research), which were anesthetized on ice for 30 min at intervals of 10 min, and isolated from the theca and follicle layers using fine forceps [29]. After 2 days, the oocytes were injected with 20 nl of Kv1.3 or Kv1.5 cRNA (0.4 μg/μl). All procedures complied with the Research Guidelines of the Kangwon National University IACUC. The injected oocytes were maintained at 17°C in modified Barth's solution containing 88 mM NaCl, 1 mM KCl, 0.4 mM CaCl$_2$, 0.33 mM Ca(NO$_3$)$_2$, 1 mM MgSO$_4$, 2.4 mM NaHCO$_3$, 10 mM HEPES (pH 7.4), and 50 μg/ml gentamicin sulfate. The currents were measured 4–5 days following cRNA injection.

Voltage clamp recording of the oocytes

Oocytes injected with Kv cRNA were perfused with ND96 solution containing 96 mM NaCl, 2 mM KCl, 1.8 mM CaCl$_2$, 1 mM MgCl$_2$, and 10 mM HEPES (pH 7.4) at a constant flow rate in an experimental bath chamber. Solution exchange required approximately 3–4 min [29]. The currents were measured 8 and 15 min after solution exchange at room temperature (20°C–23°C) using a two-microelectrode voltage clamp system (Warner Instruments). The voltage- and current-passing electrodes were filled with 3 M KCl. The resistance values for the voltage- and current-passing electrodes were 2.0–4.0 and 2.0–2.5 MΩ, respectively. Stimulation and data acquisition were controlled using a Digital 1200 AD-DA converter (Axon Instruments) with pCLAMP software (v5.1, Axon Instruments). Stock solutions of PCB77 (ChemSpider) were prepared in dimethyl sulfoxide (DMSO) and added to the ND96 solution at final concentrations of 3 nM and 10 nM shortly before each experiment. The concentration of DMSO was within 0.1%. All reagents were purchased from Sigma.

Enzyme-linked immunosorbent assay (ELISA)

Mouse Raw264.7 cells were pretreated with PCB77 (vehicle) for

24 h and stimulated with 100 ng/ml of LPS (Sigma-Aldrich) for 12 or 24 h, which is a concentration and time known to induce the release of inflammatory cytokines. Cell-free culture supernatants were collected at the indicated time points, and the TNF-α and IL-10 concentrations were measured using a development ELISA kit from PeproTech based on the manufacturer's instructions [30,31]. The absorbance values of the samples were measured at 405 nm using a microplate reader (Biotek Instruments Inc.) and converted to concentrations (pg/ml) based on the standard curves established using recombinant murine TNF-α and IL-10 (Pepro-Tech).

Data analysis

pCLAMP 10.7 (Molecular Devices) software was used for all electrophysiological analyses. The activation current traces were fitted with a single exponential function to measure the dominant time constant. Steady-state activation curves were obtained by fitting the data to the Boltzmann equation as follows:

$$y = 1/\{1 + \exp[-(V - V_{1/2})/k]\},$$

where V is the test potential, $V_{1/2}$ is the potential at half-maximal activation, and k is the slope factor. All electrophysiological data are expressed as the mean ± standard error of the mean (SEM), where n is the number of oocytes. Post-treatment current parameters were compared with corresponding baseline values using a paired sample Student's t-test with Origin 8.0 (OriginLab Corporation). The mean values of the data for the treatment group were compared using a one-way analysis of variance (ANOVA) followed by Tukey's *post-hoc* test. Differences were considered significant at $p < 0.05$ (two-tailed).
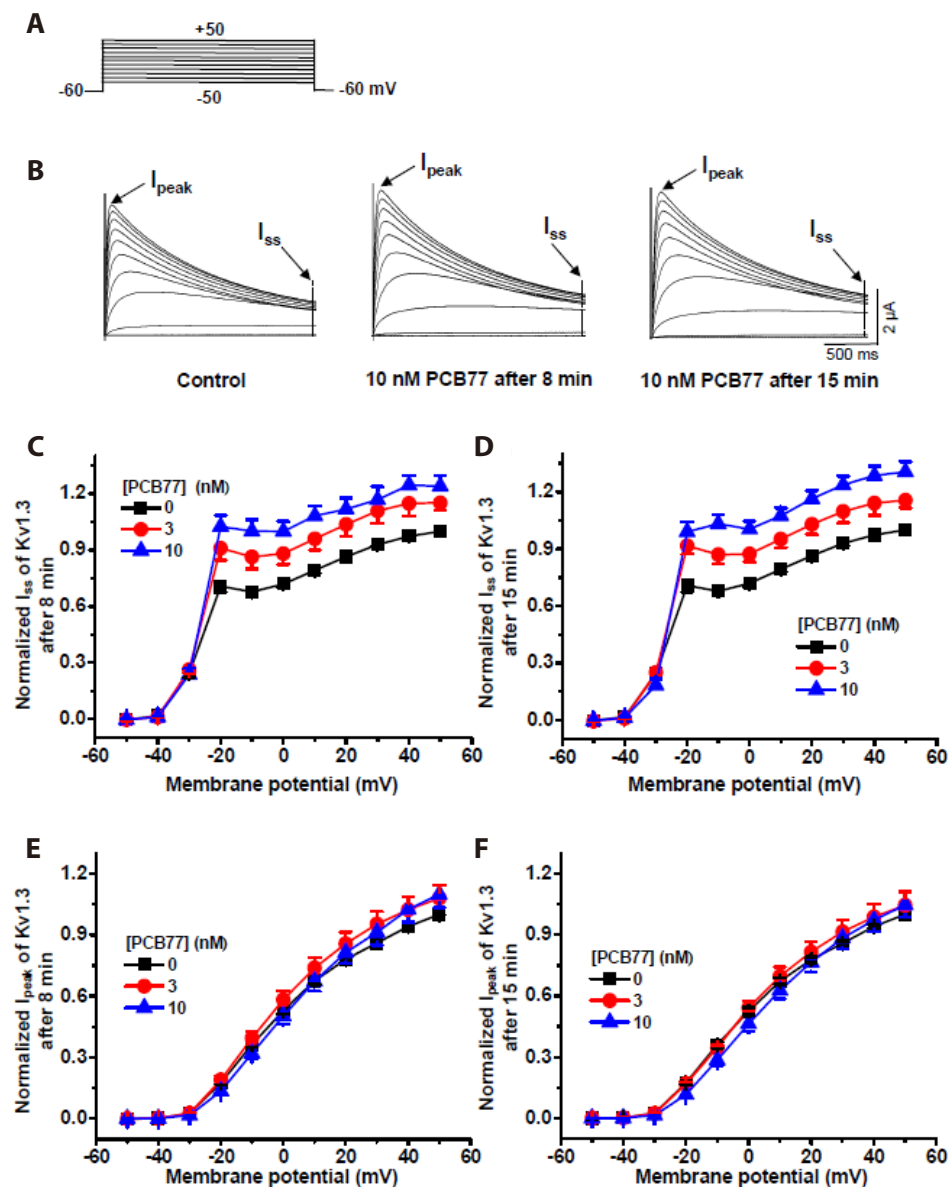

Fig. 2. 3,3',4,4'-tetrachlorobiphenyl (PCB77) enhanced human steady-state Kv1.3 currents expressed in *Xenopus* oocytes. (A) Currents were evoked by 2-s voltage pulses from a holding potential of −60 to +50 mV with an increment of 10 mV. (B) The current traces from a control oocyte and one treated with 10 nM PCB77 for 8 and 15 min. (C–F) Steady-state current–voltage (C, D) and peak current–voltage (E, F) relationships for human Kv1.3 currents in the presence of 0 (control), 3, and 10 nM PCB77 for 8 min (C, E) or 15 min (D, F). Steady-state currents were measured at the end of the 2-s pulse shown as dotted lines. Peak currents and steady-state currents were normalized to the corresponding values at +50 mV. Data are presented as the mean ± SEM (n = 4–11 oocytes per concentration group).

ELISA results are expressed as the mean ± SD of at least three independent experiments. The mean values were compared using a one-way ANOVA followed by Tukey's *post-hoc* tests for pairwise comparisons using GraphPad Prism 5 (GraphPad Software). Differences were considered significant at p < 0.05. Levels of significance are indicated by *p < 0.05, **p < 0.01, ***p < 0.001, and ns (not significant, p > 0.05).

RESULTS

PCB77 enhanced steady-state current of human Kv1.3 channel

The effects of PCB77 on hKv 1.3 channel currents were measured in *Xenopus* oocytes by two-electrode voltage clamping 4–5 days after cRNA injection (Fig. 2A, B). The currents were measured at the peak, and steady-state currents were determined at the end of the depolarizing pulses. Steady-state currents were initially recorded in ND96 solution alone and then 8 (Fig. 2C) and 15 min (Fig. 2D) after perfusion with ND96 solution containing 3 and 10 nM PCB77. The peak currents were initially recorded in ND96 solution alone and then 8 (Fig. 2E) and 15 min (Fig. 2F) after perfusion with ND96 solution containing the same concentrations of PCB77. PCB77 enhanced the steady-state current compared with ND96 alone (Fig. 2B–D) (all p < 0.05, n = 4–11 cells per concentration), with a peak effect at 10 nM PCB77 for 15 min (30.6% ± 5.4%, n = 5 oocytes per concentration, p < 0.05, Fig. 2D). However, PCB77 showed no significant effect on the peak currents of the Kv1.3 channel after 8 and 15 min of perfusion (Fig. 2B, E, and F).
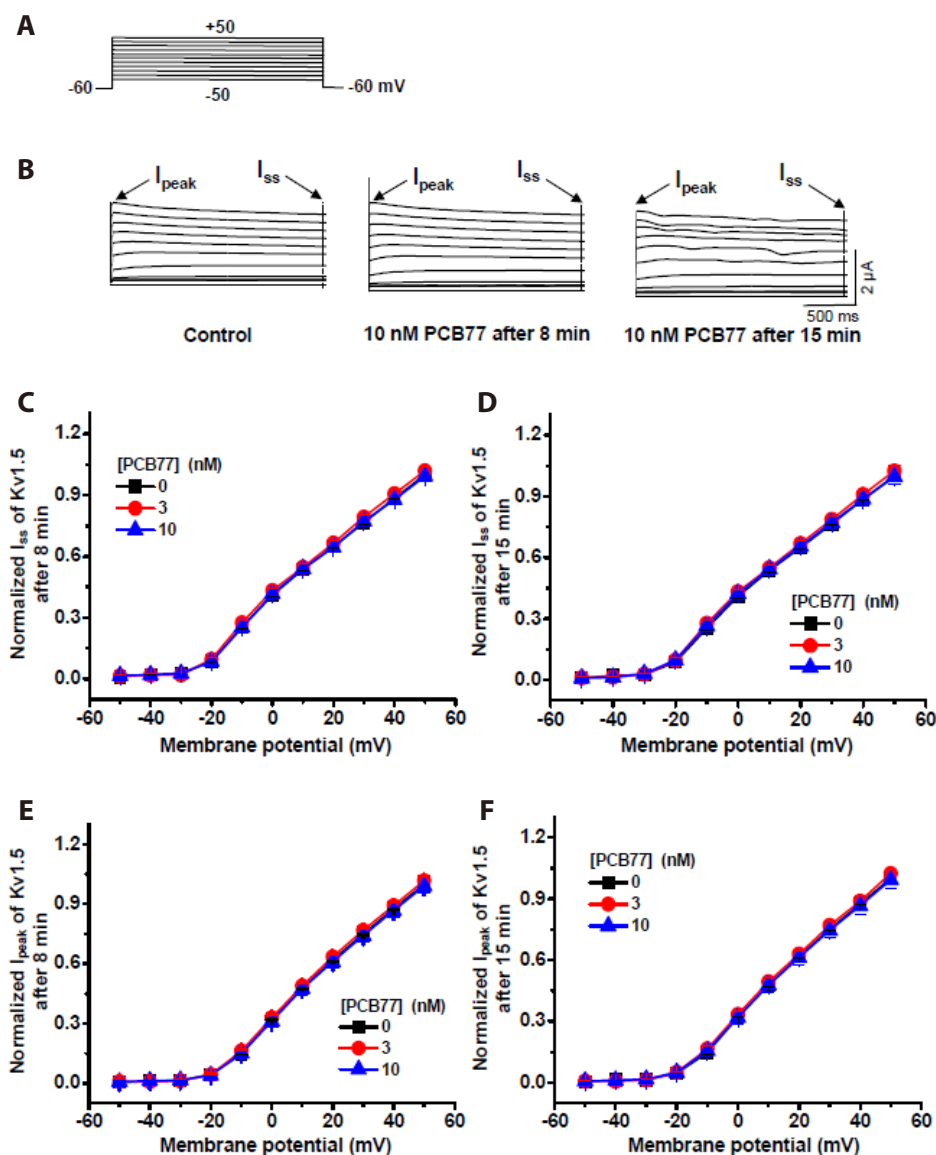

Fig. 3. 3,3′,4,4′-tetrachlorobiphenyl (PCB77) does not influence human Kv1.5 channel currents. (A) Currents were evoked in oocytes using the same voltage pulse protocol as in Fig. 2. (B) Current traces from a control oocyte and one treated with 10 nM PCB77 for 8 and 15 min. (C–F) Steady-state current–voltage (C, D) and peak current–voltage (E, F) relationships for human Kv1.5 currents in the presence of 0 (control), 3, and 10 nM PCB77 for 8 min (C, E) or 15 min (D, F). Steady-state currents were measured at the end of each 2-s depolarizing pulse shown as dotted lines. Peak and steady-state current magnitudes were normalized to the corresponding values at +50 mV. Data are presented as the mean ± SEM (n = 5–11 oocytes per concentration group).

PCB77 did not alter human Kv1.5 channel currents

The effects of PCB77 on human Kv1.5 channel currents were measured in *Xenopus* oocytes by two-electrode voltage clamping (Fig. 3A, B). The peak and steady-state currents were first recorded in ND96 solution alone and then 8 and 15 min after perfusion with ND96 solution containing 3 and 10 nM PCB77 (Fig. 3C–F). No tested concentration of PCB77 altered the steady-state or peak hKv 1.5 current after 8 or 15 min of perfusion (n = 5–11 oocytes per concentration, p > 0.05).

Comparison of the effects of PCB77 on the Kv1.3 and Kv1.5 currents

Next, we compared the effect of PCB77 on the Kv1.3 and Kv1.5 currents (Fig. 4). Its effects on the steady-state current of Kv1.3 and Kv1.5 were significantly different between the 8-min (Fig. 4A) and 15-min treatments (Fig. 4B); however, there was no difference
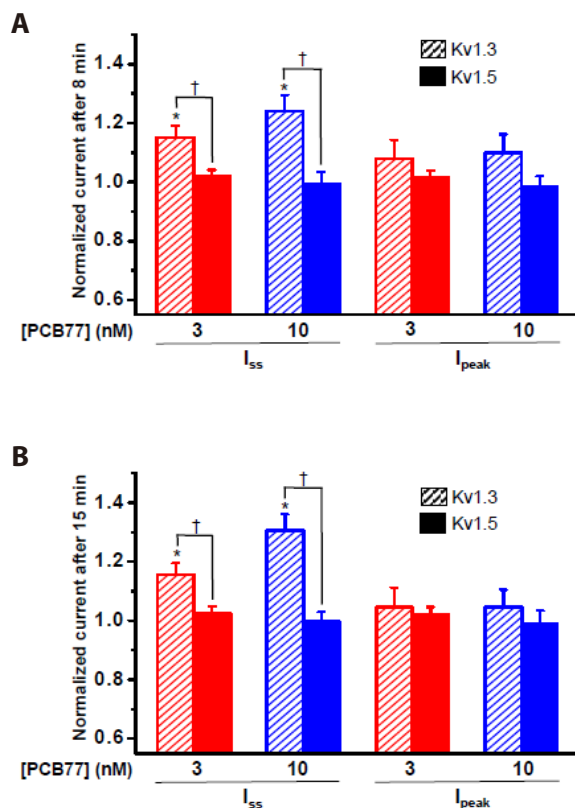
in the effects on the peak current of Kv1.3 and Kv1.5 between the 8-min (Fig. 4A) and 15-min treatments (Fig. 4B). However, there is no difference in the degree of effect of PCB77 on the steady-state current of Kv1.3 and Kv1.5 at 8-min and 15-min treatment. Therefore, even though they are from the same shaker family, Kv1.3 and Kv1.5 exhibited contrasting results in response to PCB77.

PCB77-induced enhancement of steady-state Kv1.3 current is time- and voltage-dependent

Next, the PCB77-induced increase in Kv1.3 current was compared at different command potentials (–30 to +50 mV) and treatment durations (8 and 15 min) to determine whether voltage and time dependence occurs (Fig. 5). For each depolarizing voltage step, the currents in the presence of 3 nM (Fig. 5B, C) or 10 nM PCB77 (Fig. 5D, E) for 8 and 15 min were normalized to the currents measured in the absence of PCB77. Treatment with 3 and 10 nM PCB77 for 8 min did not increase the peak or steady-state current at a test voltage of –30 mV compared with ND96 alone at the same voltage (n = 6 or 7 oocytes per treatment, all p > 0.05, Fig. 5B, D), whereas treatment for 15 min at either concentration increased the steady-state current responses to more depolarized potentials (–20 to +50 mV *vs.* –30 mV) (n = 4–7 oocytes per concentration, all p < 0.05, Fig. 5C, E). The normalized steady-state current was significantly greater at each test voltage from –20 to +50 mV after PCB77 treatment for 15 min compared with untreated controls at the same test potentials (n = 4–7, p < 0.05, Fig. 5C, E) and at –10 mV following treatment with 10 nM PCB77 for 8 min compared with untreated controls at –10 mV (n = 6, p < 0.05, Fig. 5D). In contrast, the 8-min treatment had no significant effect on the peak or steady-state current at most test potentials. These results indicate that the potentiation of steady-state current by PCB77 is strongly voltage- (between –30 and –10 mV) and time-dependent.

PCB77 treatment slows both the Kv1.3 current activation and inactivation rates

To determine whether PCB77 influences the time course of the Kv1.3 channel current, the activation and inactivation phases were fitted with single exponential functions (Fig. 6). Exposure to PCB77 for 15 min increased the activation time constant (τ) at +50 mV from 6.44 ± 0.36 ms for ND96 alone to 9.26 ± 0.34 ms in 3 nM and 12.38 ± 0.93 in 10 nM PCB77 (n = 6–11 oocytes per concentration, p < 0.05, Fig. 6A, C). Thus, submicromolar concentrations of PCB77 progressively slow the channel activation rate. Similarly, PCB77 exposure for 15 min increased the τ of inactivation at –60 mV from 591.13 ± 13.85 ms for ND96 alone to 656.01 ± 8.87 ms in 3 nM and 673.05 ± 15.85 ms in 10 nM PCB77 (n = 6–11, p < 0.05, Fig. 6B, D), indicating that PCB77 slows the inactivation velocity in a dose-dependent manner.

Fig. 4. Comparison of the effects of 3,3′,4,4′-tetrachlorobiphenyl (PCB77) on Kv1.3 and Kv1.5 currents. (A, B) Average changes in the magnitude of steady-state (I_{ss}) and peak current (I_{peak}) evoked at +50 mV by 3 and 10 nM PCB77 treatment for 8 (A) or 15 min (B) relative to the corresponding controls. Asterisks indicate significant differences between the control in the absence of PCB77 and the indicated currents in the presence of PCB77. Daggers indicate significant differences between Kv1.3 and Kv1.5 currents in the presence of PCB77. Data are presented as the mean ± SEM (n = 4–11 oocytes per concentration treatment, *,†p < 0.05).
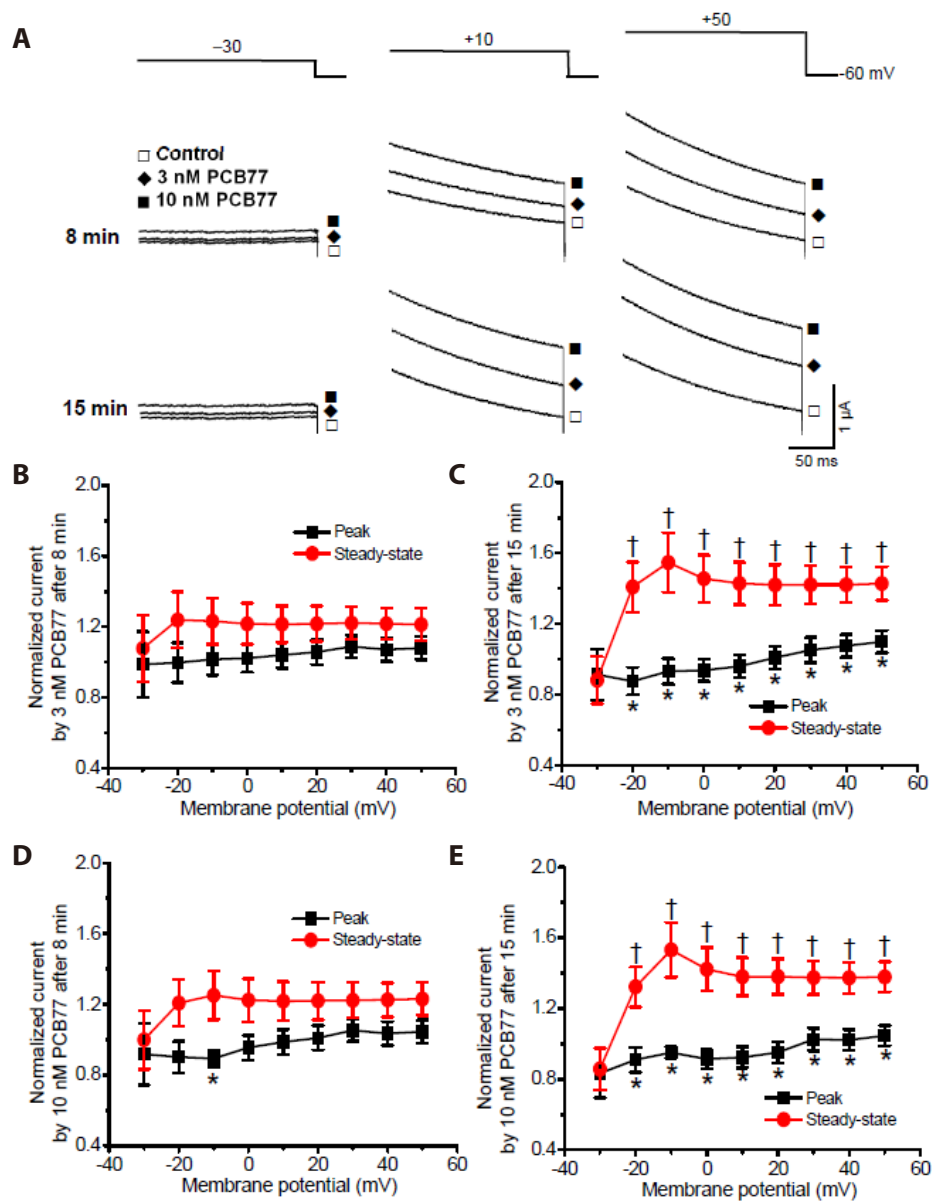
Fig. 5. Time and voltage-dependence of steady-state Kv1.3 current modulation by 3,3′,4,4′-tetrachlorobiphenyl (PCB77). (A) Current traces elicited by 2-s depolarizations of −20, +10, and +50 mV from a holding potential of −60 mV before (control) and after exposure to 3 and 10 nM PCB77. (B–E) PCB19-induced changes in peak and steady-state Kv1.3 currents at different command potentials. For each depolarizing voltage step, the current in the presence of 3 (B, C) or 10 nM PCB77 (D, E) at 8 and 15 min were normalized to the currents obtained in the absence of PCB77. Asterisks indicate significant differences between the peak and steady-state currents at each command potential in the presence of PCB77 *vs.* controls. Daggers indicate significant differences compared with the response at −30 mV. Data presented as mean ± SEM (n = 4–7 oocytes per concentration, *,†p < 0.05).

PCB77 right-shifts the Kv1.3 current steady-state activation curve but does not influence the steady-state inactivation curve

To determine whether PCB77 influences the activation kinetics of Kv1.3 channel currents, a two-pulse protocol was used to evoke the tail currents (Fig. 7). Steady-state activation curves were generated using normalized tail currents (Fig. 7B) and fitted to two different Boltzmann equations. Treatment with PCB77 for 15 min increased the half-activation potential ($V_{1/2}$) from −1.74 ± 1.26 mV in ND96 alone (n = 7) to 3.64 ± 1.18 mV in 3 nM (n = 5) and 9.44 ± 2.44 mV in 10 nM PCB77 (n = 5). Furthermore, it increased the slope factor from 13.92 ± 0.67 mV in ND96 alone (n = 7) to 14.76 ± 0.51 mV in 3 nM (n = 5) and 16.34 ± 1.09 mV in 10 nM PCB77 (n = 5) (Fig. 7C). Therefore, PCB77 significantly shifted the steady-

state activation curves of Kv1.3 toward greater depolarization (p < 0.05); however, PCB77 did not affect the steady-state inactivation kinetics at either 3 or 10 nM, as indicated by insignificant differences in $V_{1/2}$ and k values (n = 5 oocytes per concentration, Fig. 8, p > 0.05).

PCB77-induced increase in Kv1.3 current is irreversible

Next, we examined the reversibility of PCB77-mediated steady-state Kv1.3 current enhancement following washout. Although the increase in steady-state current induced by 10 nM PCB77 exhibited a relatively rapid onset, the effect lasted for ≥ 40 min following washout (n = 3 cells, Fig. 9). In addition, the normalized steady-state current magnitude was still markedly higher after washout compared with that of the normalized steady-state cur-
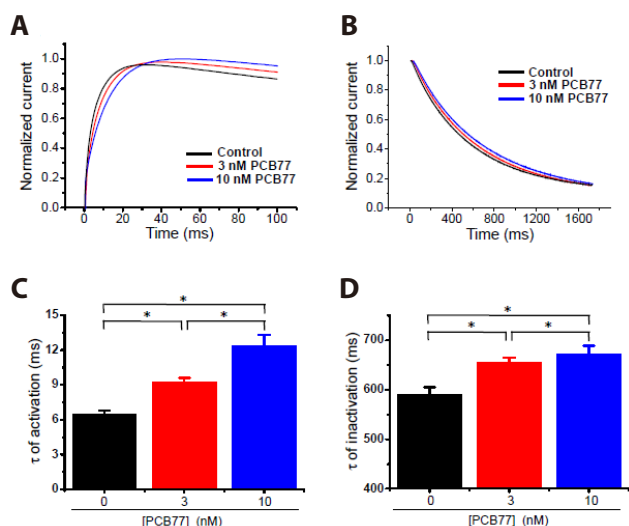
Fig. 6. Slowing of Kv1.3 current kinetics by 3,3′,4,4′-tetrachlorobi-phenyl (PCB77). The time constants of current activation and inactivation were estimated by fitting each exponential function to traces evoked by a single +50 mV pulse for a 2-s duration from a holding potential of −60 mV. (A) Representative normalized current traces of the activation phase in the absence of PCB77 (dark) and the presence of 3 and 10 nM PCB77 for 15 min (colored). Each current trace was normalized to its peak value. (B) Representative normalized current traces for the inactivation phase in the absence of PCB77 and in the presence of 3 and 10 nM PCB77 for 15 min. (C, D) Summary of the activation time constants (C) and inactivation time constants (D). Data are presented as the mean ± SEM (n = 6–11 oocytes per concentration, *p < 0.05).

rents recorded for the same duration in the absence of PCB77 (Fig. 9). These results suggest that PCB77 enhances steady-state human Kv1.3 currents through an intracellular signaling mechanism, possibly involving long-lasting post-translational modifications.

Activation of the Kv1.3 current by PCB77 negatively regulates LPS-induced inflammatory responses in mouse macrophages

The Kv1.3 channel is activated by an increase in intracellular Ca^{2+} concentration, which is the same signal responsible for T-cell activation [20]. In addition, several studies have concluded that the Kv1.3 channel is a potential therapeutic target for various autoimmune diseases and cancers [32,33]. Thus, the Kv1.3 current may modulate T-cell immune function; however, the function of the Kv1.3 channel in macrophages and monocytes is not fully understood. Therefore, we examined whether the Kv1.3 channel modulates the immune response in Raw264.7 cells, a mouse monocyte/macrophage cell line. Treatment with PCB77 increased the production of the proinflammatory cytokine TNF-α (Fig. 10A, left), whereas anti-inflammatory cytokine IL-10 production was reduced in a dose-dependent manner (Fig. 10A, right). LPS is a major component of the gram-negative bacterial cell wall and can induce acute and severe inflammatory responses by enhanc-
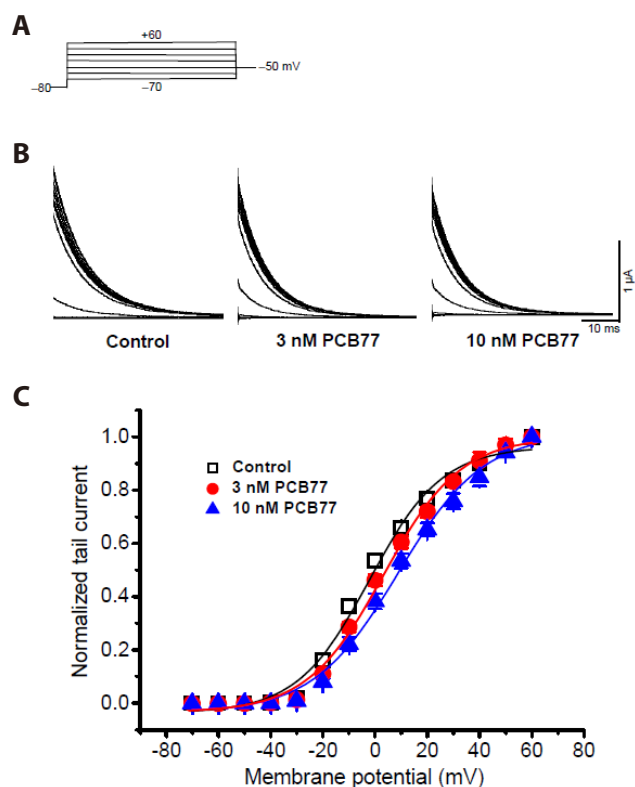

Fig. 7. 3,3′,4,4′-tetrachlorobiphenyl (PCB77) shifts the steady-state Kv1.3 current activation curve to more depolarized potentials. (A, B) Representative steady-state activation tail currents recorded at −50 mV after 100 ms of depolarizing pulses from −70 to +60 mV in the absence and presence of 3 and 10 nM PCB77. (C) Steady-state activation curves were obtained by normalizing each tail current to the traces evoked at +60 mV and by fitting the data to the Boltzmann equation. Data are presented as the mean ± SEM (n = 5–7 oocytes per treatment).

ing the secretion of multiple inflammatory cytokines from various cell types. Because LPS is widely used as a potent activator of immune cells, such as monocytes and macrophages, Raw264.7 cells were stimulated with LPS in the presence of PCB77 to mimic gram-negative bacteria infection under continuous exposure to PCB77. In contrast to treatment with PCB77 alone, PCB77 suppressed the production of TNF-α and IL-10 in Raw264.7 cells following LPS exposure (Fig. 10B). These data suggest that the activation of Kv1.3 by PCB77 treatment dysregulates the normal LPS-induced inflammatory response in mouse macrophages.

DISCUSSION

The PCB77 congener examined in the present study reduces thyroid function, induces uterine and breast tumors, and inhibits humoral and cellular immunity, in part, through AhR activation [6,8-10]. Exposure to PCBs *in utero* causes cardiac enlargement, ventricular hypertrophy, and disruption of the transcriptional programs required for normal cardiac development [34]. We
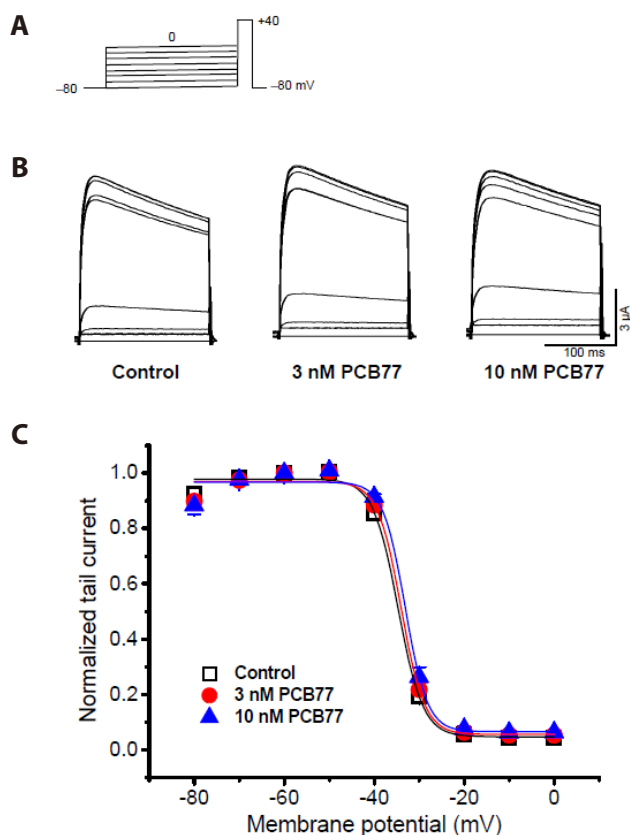
Fig. 8. 3,3′,4,4′-tetrachlorobiphenyl (PCB77) does not affect steady-state Kv1.3 current inactivation. (A) Typical tail currents elicited by depolarizing pulses from 30 s preconditioning potentials of −80–0 to +40 mV. (B) Superimposed steady-state inactivation currents in the presence of 0 (control), 3, and 10 nM PCB77. (C) Steady-state inactivation current amplitudes were normalized to those evoked from a preconditioning potential of −60 mV. The data were fitted to the Boltzmann equation to generate the steady-state inactivation curves for each condition. Data are presented as the mean ± SEM (n = 5 oocytes per concentration).

Fig. 9. Potentiating effects of 3,3′,4,4′-tetrachlorobiphenyl (PCB77) on Kv1.3 current are irreversible. Currents were evoked by a 200 ms depolarizing pulse to +60 mV from a holding potential of −60 mV at 10 s intervals before exposure to PCB77 (baseline), during the application of 10 nM PCB77, and washout. Steady-state currents were normalized to the baseline values. Normalized currents during PCB77 washout were compared with currents evoked in untreated oocytes after the same recording duration (n = 3 oocytes per treatment).
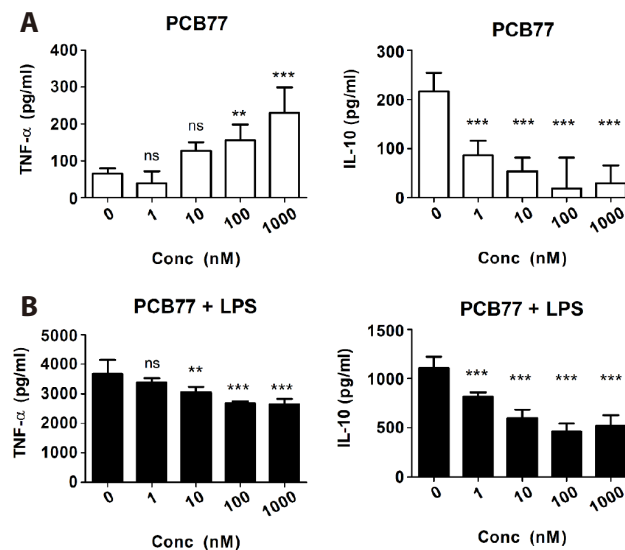
Fig. 10. 3,3′,4,4′-tetrachlorobiphenyl (PCB77) inhibits lipopolysaccharide-induced production of tumor necrosis factor-α (TNF-α) and interleukin-10 (IL-10) in mouse macrophages. (A) Raw264.7 cells were treated with PCB77 (10 μM) for 12 or 24 h. The release rates of TNF-α and IL-10 into the culture supernatant were measured using an enzyme-linked immunosorbent assay (ELISA). (B) Raw264.7 cells were pretreated with PCB77 for 24 h and then stimulated with lipopolysaccharide (LPS) for 12 or 24 h. The release rates of TNF-α and IL-10 into the culture supernatant were measured using an ELISA. All experiments were performed in triplicate and compared with a one-way analysis of variance followed by Tukey's *post-hoc* test for multiple comparisons; **p < 0.01; ***p < 0.001, and not significant (ns) (p > 0.05).

demonstrated that PCB77 did not modulate the hKv 1.5 channel current, which is important for cardiac action potential repolarization (Fig. 3); however, it enhanced the steady-state hKv 1.3 current playing an important role in various immune cells at submicromolar concentrations (as low as 3–10 nM) and exposure durations as short as 8–15 min (Fig. 2). These effects were markedly dependent upon membrane voltage and exposure time (Fig. 5). Thus, exposure to trace PCB77 may disrupt normal immune function with complex dependence on exposure level and duration. Consistently, low doses of PCB77 attenuated cytokine signaling in quiescent and LPS-activated macrophages *in vitro* (Fig. 10). This suggests that these effects on human immune cells contribute to the known immunotoxicity of this compound.

In this study, PCB77, a DL-PCB with AhR affinity, acutely increased the steady-state currents of the Kv1.3 channel in a concentration-dependent manner within 8 min (Figs. 2 and 4). This acute and dose-dependent effect of PCB77 on hKv1.3 chan-
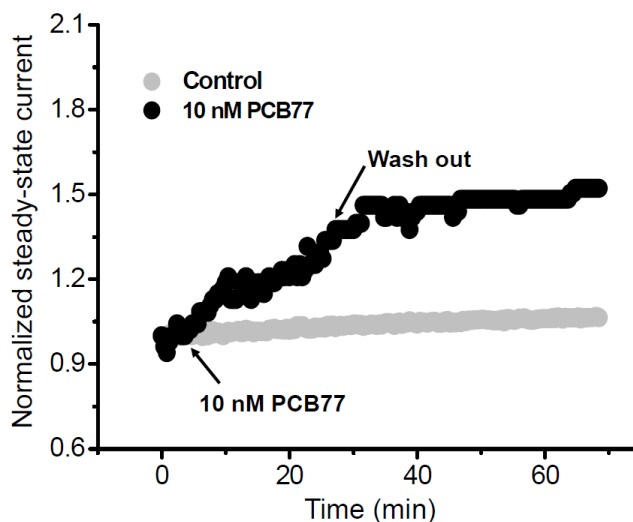
nel currents can exclude the possibility of both genomic regulations that requires more than several hours and nonspecific effects without concentration-dependency. The PCB77-induced enhancement of the Kv1.3 peak current was voltage-dependent (Fig. 5). PCB77 increased the steady-state current of the Kv1.3 channel to a greater extent compared with the peak current at the same test voltage (Fig. 5), indicating that PCB77 affected the Kv1.3 channel in an open, rather than closed state. Furthermore, the velocity of ultra-rapid activation was inhibited (Fig. 6), and the activation curves were right-shifted following PCB77 treatment (Fig. 7). These results indicate that PCB77 primarily alters channel opening. The results shown in Fig. 9 show the lack of reversibility in the enhancement of the steady-state current despite washing for > 40 min. This indicates that the lipophilic properties of PCB77 enable the drug to cross the plasma membrane and activate the Kv1.3 channel directly or indirectly through intracellular signals. Otherwise, PCB77 may induce long-lasting post-translational modifications, such as phosphorylation.

In contrast to DL-PCB PCB77, non-DL-PCB PCB19 irreversibly inhibited the Kv1.3 peak current, but did not affect the steady-state current [35]. Furthermore, PCB19 showed contrasting effects on the Kv1.3 or Kv1.5 channels, which were similar to those of PCB77 (Figs. 2–4). Considering that the distinct responses of the two channels to PCB77 may be the result of differences in their biophysical properties or blocker sensitivity, despite both channels belonging to the Kv1 Shaker family [15], we found that PCB77 acts as a selective activator of the Kv1.3 channel. We previously reported that another non-ortho DL-PCB, PCB126, also right-shifted the Kv1.3 activation curve; however, it did not affect the peak and steady-state current amplitudes of either the Kv1.3 or Kv1.5 channels [36]. These distinct profiles further underscore the functional heterogeneity of PCBs. Both PCB77 and PCB126 exhibit high affinity for AhR [37,38], suggesting that the observed effects on the Kv1.3 channel in the present study are independent of AhR binding.

PCB77 concentrations in the lower parts per million (ppm) range were detected in the blubber of five harbor seals and one harbor porpoise caught in the North Sea [39]. Serum concentrations of 331 ng/g and lipid concentrations of 2,600 ng/g have also been measured in American females [40], which are comparable to 1.1–8.9 μM PCB77. This is markedly higher than the minimum effective dose of PCB77 in the present study using *Xenopus* oocytes and the range for attenuating steady-state Kv1.3 current enhancement. Furthermore, approximately 10-fold higher concentrations of a particular receptor/channel regulator may be required to elicit the same response in *Xenopus* oocytes compared with cells exhibiting endogenous expression [29,41]. In this study, PCB77 showed the strongest effect on the steady-state Kv1.3 current amplitude and kinetics at 3 and 10 nM (Figs. 4 and 6), further underscoring the potential effect of PCB77 on Kv1.3 channel activity and its associated adverse effects.

Several studies have shown that Kv1.3 channels can not only control the proliferation, migration, and activation of T cells, microglia, and vascular smooth muscle cells, but also enhance or attenuate inflammatory responses depending on the immune cell type [22,28,42]. The Kv1.3 channel regulates membrane potential and calcium signals in T cells [43], neurons, and microglia [21]. An increase in the activity of the Kv1.3 channel can enhance T-cell reactivity and cause inflammatory tissue destruction [21], whereas increased Kv1.3 activity in B cells, macrophages, and microglia may result in the development of autoimmune diseases [21]. Kan *et al*. [44] demonstrated that Kv1.3 channels contribute to macrophage migration in atherosclerosis by upregulating extracellular signal-regulated kinase (ERK) activity. Zhu *et al*. [27] demonstrated that blocking the Kv1.3 channel with *Stichodactyla helianthus* neurotoxin enhanced the phagocytic capacity of macrophages. The Kv1.3 channel blocks membrane depolarization and modulates Ca^{2+} activation signaling by effluxing K^+, leading to T-cell proliferation and cytokine production [45,46]. PCB77 also increased the production of the proinflammatory cytokine TNF-α in quiescent macrophages in a dose-dependent manner and decreased the production of the anti-inflammatory cytokine IL-10 (Fig. 10). These results are consistent with those of previous studies, in which Kv1.3 knockout microglia reduces the secretion of proinflammatory cytokines, such as TNF and IL-1β, in LPS-stimulated cells [28]. However, pretreatment with PCB77 suppressed the production of both cytokines in LPS-stimulated mouse macrophages (Fig. 10). These results suggest that PCB77-induced activation of Kv1.3 promotes inflammation and attenuates the secretion of inflammatory mediators during some pathogenic bacterial infections or severe inflammation. Thus, endocrine disruptors, such as PCB77, persistently interfere with the activity of the immune system, preventing the immune response from becoming activated following exposure to gram-negative bacteria, such as *Escherichia coli* and *Salmonella*. In addition, these results suggest that PCB77-induced enhancement of Kv1.3 inhibits cytokine production in activated macrophages, which is consistent with several previous studies [47,48]. Collectively, although PCB77 activates the Kv1.3 channel, our results indicate that PCB77 regulates the production of inflammatory cytokines through K^+ channel modulation of cytokine production in macrophages during infection by various pathogens or severe inflammation. Additional experiments involving Kv channel modulation by PCB77 or using cell models with altered Kv expression could help elucidate the relationship between PCB77 and Kv1.3 channel.

In conclusion, PCB77 rapidly increased the steady-state human Kv1.3 channel current at relatively low concentrations. We hypothesize that the increase in Kv1.3 current by PCB77 is mediated by an indirect mechanism, such as protein kinase signaling. In addition, our results suggest that the increase in Kv1.3 channel current by PCB77 exposure could cause an immune disturbance by dysregulating TNF-α and IL-10. Therefore, the persistent organic pollutant PCB77 may disturb multiple human physi-

ological functions, including the immune system, during acute and chronic exposure conditions. Further experiments including the direct measurement of membrane potential and intracellular Ca^{2+} concentration by PCB77 in immune cell will be necessary to reveal that possibility.

FUNDING

ACKNOWLEDGEMENTS

CONFLICTS OF INTEREST

The authors declare no conflicts of interest.

REFERENCES

1. Carpenter DO. Polychlorinated biphenyls (PCBs): routes of exposure and effects on human health. *Rev Environ Health*. 2006;21:1-23.

2. McFarland VA, Clarke JU. Environmental occurrence, abundance, and potential toxicity of polychlorinated biphenyl congeners: considerations for a congener-specific analysis. *Environ Health Perspect*. 1989;81:225-239.

3. Borja J, Taleon DM, Auresenia J, Gallardo S. Polychlorinated biphenyls and their biodegradation. *Process Biochem*. 2005;40:1999-2013.

4. Jacobson JL, Jacobson SW, Humphrey HE. Effects of in utero exposure to polychlorinated biphenyls and related contaminants on cognitive functioning in young children. *J Pediatr*. 1990;116:38-45.

5. Carpenter DO. Polychlorinated biphenyls and human health. *Int J Occup Med Environ Health*. 1998;11:291-303.

6. van den Berg KJ, Zurcher C, Brouwer A. Effects of 3,4,3',4'-tetrachlorobiphenyl on thyroid function and histology in marmoset monkeys. *Toxicol Lett*. 1988;41:77-86.

7. Sánchez-Alonso JA, López-Aparicio P, Recio MN, Pérez-Albarsanz MA. Apoptosis-mediated neurotoxic potential of a planar (PCB 77) and a nonplanar (PCB 153) polychlorinated biphenyl congeners in neuronal cell cultures. *Toxicol Lett*. 2003;144:337-349.

8. Ramamoorthy K, Gupta MS, Sun G, McDougal A, Safe SH. 3,3'4,4'-Tetrachlorobiphenyl exhibits antiestrogenic and antitumorigenic activity in the rodent uterus and mammary cells and in human breast cancer cells. *Carcinogenesis*. 1999;20:115-123.

9. Silkworth JB, Antrim L, Kaminsky LS. Correlations between polychlorinated biphenyl immunotoxicity, the aromatic hydrocarbon locus, and liver microsomal enzyme induction in C57BL/6 and DBA/2 mice. *Toxicol Appl Pharmacol*. 1984;75:156-165.

10. Yilmaz B, Sandal S, Chen CH, Carpenter DO. Effects of PCB 52 and PCB 77 on cell viability, [Ca(2+)](i) levels and membrane fluidity in mouse thymocytes. *Toxicology*. 2006;217:184-193.

11. Kerkvliet NI, Steppan LB, Brauner JA, Deyo JA, Henderson MC, Tomar RS, Buhler DR. Influence of the Ah locus on the humoral immunotoxicity of 2,3,7,8-tetrachlorodibenzo-p-dioxin: evidence for Ah-receptor-dependent and Ah-receptor-independent mechanisms of immunosuppression. *Toxicol Appl Pharmacol*. 1990;105:26-36.

12. Lavoie ET, Grasman KA. Effects of in ovo exposure to PCBs 126 and 77 on mortality, deformities and post-hatch immune function in chickens. *J Toxicol Environ Health A*. 2007;70:547-558.

13. Rudy B. Diversity and ubiquity of K channels. *Neuroscience*. 1988;25:729-749.

14. Felipe A, Vicente R, Villalonga N, Roura-Ferrer M, Martínez-Mármol R, Solé L, Ferreres JC, Condom E. Potassium channels: new targets in cancer therapy. *Cancer Detect Prev*. 2006;30:375-385.

15. Comes N, Bielanska J, Vallejo-Gracia A, Serrano-Albarrás A, Marruecos L, Gómez D, Soler C, Condom E, Ramón Y Cajal S, Hernández-Losa J, Ferreres JC, Felipe A. The voltage-dependent K(+) channels Kv1.3 and Kv1.5 in human cancer. *Front Physiol*. 2013;4:283.

16. Feng J, Wible B, Li GR, Wang Z, Nattel S. Antisense oligodeoxynucleotides directed against Kv1.5 mRNA specifically inhibit ultrarapid delayed rectifier K+ current in cultured adult human atrial myocytes. *Circ Res*. 1997;80:572-579.

17. Decher N, Pirard B, Bundis F, Peukert S, Baringhaus KH, Busch AE, Steinmeyer K, Sanguinetti MC. Molecular basis for Kv1.5 channel block: conservation of drug binding sites among voltage-gated K+ channels. *J Biol Chem*. 2004;279:394-400.

18. Honoré E, Barhanin J, Attali B, Lesage F, Lazdunski M. External blockade of the major cardiac delayed-rectifier K+ channel (Kv1.5) by polyunsaturated fatty acids. *Proc Natl Acad Sci U S A*. 1994;91:1937-1941.

19. Olson TM, Alekseev AE, Liu XK, Park S, Zingman LV, Bienengraeber M, Sattiraju S, Ballew JD, Jahangir A, Terzic A. Kv1.5 channelopathy due to KCNA5 loss-of-function mutation causes human atrial fibrillation. *Hum Mol Genet*. 2006;15:2185-2191.

20. Wei AD, Gutman GA, Aldrich R, Chandy KG, Grissmer S, Wulff H. International Union of Pharmacology. LII. Nomenclature and molecular relationships of calcium-activated potassium channels. *Pharmacol Rev*. 2005;57:463-472.

21. Pérez-Verdaguer M, Capera J, Serrano-Novillo C, Estadella I, Sastre D, Felipe A. The voltage-gated potassium channel Kv1.3 is a promising multitherapeutic target against human pathologies. *Expert Opin Ther Targets*. 2016;20:577-591.

22. Pérez-García MT, Cidad P, López-López JR. The secret life of ion channels: Kv1.3 potassium channels and proliferation. *Am J Physiol Cell Physiol*. 2018;314:C27-C42.

23. Wulff H, Calabresi PA, Allie R, Yun S, Pennington M, Beeton C, Chandy KG. The voltage-gated Kv1.3 K(+) channel in effector memory T cells as new target for MS. *J Clin Invest*. 2003;111:1703-1713. Erratum in: *J Clin Invest*. 2003;112:298.

24. Hu L, Pennington M, Jiang Q, Whartenby KA, Calabresi PA. Characterization of the functional properties of the voltage-gated potas-

sium channel Kv1.3 in human CD4+ T lymphocytes. *J Immunol*. 2007;179:4563-4570.

25. Knaus HG, McManus OB, Lee SH, Schmalhofer WA, Garcia-Calvo M, Helms LM, Sanchez M, Giangiacomo K, Reuben JP, Smith AB 3rd, Kaczorowski GJ, Garcia ML. Tremorgenic indole alkaloids potently inhibit smooth muscle high-conductance calcium-activated potassium channels. *Biochemistry*. 1994;33:5819-5828.

26. Cahalan MD, Chandy KG. Ion channels in the immune system as targets for immunosuppression. *Curr Opin Biotechnol*. 1997;8:749-756.

27. Zhu H, Yan L, Gu J, Hao W, Cao J. Kv1.3 channel blockade enhances the phagocytic function of RAW264.7 macrophages. *Sci China Life Sci*. 2015;58:867-875.

28. Di Lucente J, Nguyen HM, Wulff H, Jin LW, Maezawa I. The voltage-gated potassium channel Kv1.3 is required for microglial pro-inflammatory activation in vivo. *Glia*. 2018;66:1881-1895.

29. Jo SH, Hong HK, Chong SH, Won KH, Jung SJ, Choe H. Clomipramine block of the hERG K+ channel: accessibility to F656 and Y652. *Eur J Pharmacol*. 2008;592:19-25.

30. Lee HJ, Kang SJ, Woo Y, Hahn TW, Ko HJ, Jung YJ. TLR7 stimulation with imiquimod induces selective autophagy and controls *Mycobacterium tuberculosis* growth in mouse macrophages. *Front Microbiol*. 2020;11:1684.

31. Mohammad HMF, El-Baz AA, Mahmoud OM, Khalil S, Atta R, Imbaby S. Protective effects of evening primrose oil on behavioral activities, nigral microglia and histopathological changes in a rat model of rotenone-induced parkinsonism. *J Chem Neuroanat*. 2023;127:102206.

32. Serrano-Albarrás A, Estadella I, Cirera-Rocosa S, Navarro-Pérez M, Felipe A. Kv1.3: a multifunctional channel with many pathological implications. *Expert Opin Ther Targets*. 2018;22:101-105.

33. Teisseyre A, Palko-Labuz A, Sroda-Pomianek K, Michalak K. Voltage-gated potassium channel Kv1.3 as a target in therapy of cancer. *Front Oncol*. 2019;9:933.

34. Kang JA, Park SH, Jeong SP, Han MH, Lee CR, Lee KM, Kim N, Song MR, Choi M, Ye M, Jung G, Lee WW, Eom SH, Park CS, Park SG. Epigenetic regulation of Kcna3-encoding Kv1.3 potassium channel by cereblon contributes to regulation of CD4+ T-cell activation. *Proc Natl Acad Sci U S A*. 2016;113:8771-8776.

35. Kim JH, Hwang S, Jo SH. Non-dioxin-like polychlorinated biphenyl 19 has distinct effects on human Kv1.3 and Kv1.5 channels. *Toxicol Appl Pharmacol*. 2021;411:115365.

36. Kim JH, Hwang S, Park SI, Jo SH. Effects of 3, 3, 4, 4, 5-pentachlo-

robiphenyl on human Kv1.3 and Kv1.5 channels. *Int J Oral Biol*. 2019;44:115-123.

37. Poland A, Knutson JC. 2,3,7,8-tetrachlorodibenzo-p-dioxin and related halogenated aromatic hydrocarbons: examination of the mechanism of toxicity. *Annu Rev Pharmacol Toxicol*. 1982;22:517-554.

38. Dean KM, Marcell AM, Baltos LD, Carro T, Bohannon MEB, Ottinger MA. Comparative lethality of in ovo exposure to PCB 126, PCB 77, and 2 environmentally relevant PCB mixtures in Japanese Quail (Coturnix japonica). *Environ Toxicol Chem*. 2019;38:2637-2650.

39. Beck H, Breuer EM, Droß A, Mathar W. Residues of PCDDs, PCDFs, PCBs and other organochlorine compounds in harbour seals and harbour porpoise. *Chemosphere*. 1990;20:1027-1034.

40. Zhang Y, Wise JP, Holford TR, Xie H, Boyle P, Zahm SH, Rusiecki J, Zou K, Zhang B, Zhu Y, Owens PH, Zheng T. Serum polychlorinated biphenyls, cytochrome P-450 1A1 polymorphisms, and risk of breast cancer in Connecticut women. *Am J Epidemiol*. 2004;160:1177-1183.

41. Choi SY, Koh YS, Jo SH. Inhibition of human ether-a-go-go-related gene K+ channel and IKr of guinea pig cardiomyocytes by antipsychotic drug trifluoperazine. *J Pharmacol Exp Ther*. 2005;313:888-895.

42. Serrano-Novillo C, Capera J, Colomer-Molera M, Condom E, Ferreres JC, Felipe A. Implication of voltage-gated potassium channels in neoplastic cell proliferation. *Cancers (Basel)*. 2019;11:287.

43. Lewis RS, Cahalan MD. Potassium and calcium channels in lymphocytes. *Annu Rev Immunol*. 1995;13:623-653.

44. Kan XH, Gao HQ, Ma ZY, Liu L, Ling MY, Wang YY. Kv1.3 potassium channel mediates macrophage migration in atherosclerosis by regulating ERK activity. *Arch Biochem Biophys*. 2016;591:150-156.

45. Wulff H, Castle NA, Pardo LA. Voltage-gated potassium channels as therapeutic targets. *Nat Rev Drug Discov*. 2009;8:982-1001.

46. Wang X, Li G, Guo J, Zhang Z, Zhang S, Zhu Y, Cheng J, Yu L, Ji Y, Tao J. Kv1.3 channel as a key therapeutic target for neuroinflammatory diseases: state of the art and beyond. *Front Neurosci*. 2020;13:1393. Erratum in: *Front Neurosci*. 2020;14:163.

47. Villalonga N, David M, Bielanska J, Vicente R, Comes N, Valenzuela C, Felipe A. Immunomodulation of voltage-dependent K+ channels in macrophages: molecular and biophysical consequences. *J Gen Physiol*. 2010;135:135-147.

48. Vaeth M, Feske S. Ion channelopathies of the immune system. *Curr Opin Immunol*. 2018;52:39-50.